IAI Journals.ASM.org

Motor Rotation Is Essential for the Formation of the Periplasmic Flagellar Ribbon, Cellular Morphology, and *Borrelia burgdorferi* Persistence within *Ixodes scapularis* Tick and Murine Hosts

Syed Z. Sultan,[a] Padmapriya Sekar,[b] Xiaowei Zhao,[c] Akarsh Manne,[a] Jun Liu,[c] R. Mark Wooten,[b] M. A. Motaleb[a]

Department of Microbiology and Immunology, Brody School of Medicine, East Carolina University, Greenville, North Carolina, USA[a]; Department of Medical Microbiology and Immunology, University of Toledo College of Medicine, Toledo, Ohio, USA[b]; Department of Pathology and Laboratory Medicine, University of Texas Medical School at Houston, Houston, Texas, USA[c]

***Borrelia burgdorferi* must migrate within and between its arthropod and mammalian hosts in order to complete its natural enzootic cycle. During tick feeding, the spirochete transmits from the tick to the host dermis, eventually colonizing and persisting within multiple, distant tissues. This dissemination modality suggests that flagellar motor rotation and, by extension, motility are crucial for infection. We recently reported that a nonmotile *flaB* mutant that lacks periplasmic flagella is rod shaped and unable to infect mice by needle or tick bite. However, those studies could not differentiate whether motor rotation or merely the possession of the periplasmic flagella was crucial for cellular morphology and host persistence. Here, we constructed and characterized a *motB* mutant that is nonmotile but retains its periplasmic flagella. Even though Δ*motB* bacteria assembled flagella, part of the mutant cell is rod shaped. Cryoelectron tomography revealed that the flagellar ribbons are distorted in the mutant cells, indicating that motor rotation is essential for spirochetal flat-wave morphology. The Δ*motB* cells are unable to infect mice, survive in the vector, or migrate out of the tick. Coinfection studies determined that the presence of these nonmotile Δ*motB* cells has no effect on the clearance of wild-type spirochetes during murine infection and vice versa. Together, our data demonstrate that while flagellar motor rotation is necessary for spirochetal morphology and motility, the periplasmic flagella display no additional properties related to immune clearance and persistence within relevant hosts.**

Borrelia burgdorferi, the Lyme disease spirochete, shuttles principally between the *Ixodes* ticks and a vertebrate host during its natural infection cycle (1–5). In the tick, spirochetes reside primarily in the midgut until the introduction of the host blood meal. During tick feeding on a vertebrate host, spirochetes replicate, and a subset of the motile organisms cross the midgut epithelium into the hemocoel before reaching the salivary glands, where they subsequently are deposited into the host dermis (6–8). Once in the host, *B. burgdorferi* must migrate through the complex skin tissues, including some hematogenous dissemination, and eventually colonize distant tissues, where they often produce disease symptoms in certain hosts. Subsequently, when a naive tick feeds on an infected reservoir host, spirochetes in the skin migrate into the arthropod to complete the enzootic cycle (3, 4, 9). During the spirochete's migration within and between the hosts, periplasmic flagellar motor rotation and, by extension, motility are thought to be crucial for infection (10, 11). Indeed, nonmotile, reduced-motility, or nonchemotactic mutant spirochetes were found to be attenuated in mouse infection (12–14). Additionally, our data indicate that *B. burgdorferi* remains constantly motile in the mouse dermis, even 2 years after needle inoculation (P. Sekar, R. M. Wooten, and M. A. Motaleb, unpublished results). In fact, this Lyme disease spirochete can swim at speeds that are many times faster than that recorded for any skin-resident host immune cells (15, 16, and R. M. Wooten, unpublished results). These findings suggest that spirochetal motility is an important factor for both initial dissemination and long-term persistence within the mammalian host.

Bacterial flagella have been studied extensively in *Escherichia coli* and *Salmonella enterica* serovar Typhimurium (17). The flagella are driven by ion infiltration through the membrane-bound stator complex MotA-MotB, also known as the torque-generating units (18–20). Amino acid sequence analysis of *B. burgdorferi* MotA and MotB indicates that they share 24% and 45% identity, respectively, with those in *E. coli* (21). Genome sequence analyses as well as cryoelectron tomography (cryo-ET) data suggest that spirochetal periplasmic flagella are similar to *E. coli* flagella in many aspects (22–24), although the regulation of motility and chemotaxis genes are distinctive (11, 25). While *B. burgdorferi* motility and chemotaxis genes identified to date are transcribed by the housekeeping σ^{70} factor of RNA polymerase, those genes in *E. coli* are regulated in a hierarchical manner (11, 25, 26). A periplasmic flagellum is composed of at least 50 proteins that can be subdivided into three major parts: the basal body-motor-switch complex, the hook, and the filament (24, 27).

B. burgdorferi normally exhibits flat-wave morphology and has unique modes of motility (10, 11, 28). Wild-type cells run, pause,

Received 17 December 2014 **Returned for modification** 27 January 2015
Accepted 5 February 2015

Accepted manuscript posted online 17 February 2015

Citation Sultan SZ, Sekar P, Zhao X, Manne A, Liu J, Wooten RM, Motaleb MA. 2015. Motor rotation is essential for the formation of the periplasmic flagellar ribbon, cellular morphology, and *Borrelia burgdorferi* persistence within *Ixodes scapularis* tick and murine hosts. Infect Immun 83:1765–1777. doi:10.1128/IAI.03097-14.

Editor: A. Camilli

Address correspondence to M. A. Motaleb, motalebm@ecu.edu.

Supplemental material for this article may be found at http://dx.doi.org/10.1128/IAI.03097-14.

doi:10.1128/IAI.03097-14

or flex, and then they run in a new direction or reverse. These modes of motility (run, flex, and reverse) are believed to be achieved as this spirochete's flagella rotate asymmetrically (11, 29). For an individual bacterium, 7 to 11 periplasmic flagella are attached to each pole of the cell and extend toward the middle of the cell as they wrap around the cell cylinder (30–32). Periplasmic flagellar filaments form a ribbon-like pattern, and those organelles are essential for the spirochetal flat-wave morphology and motility (14, 28, 32–35). As some studies have demonstrated that motility and chemotaxis are crucial for spirochetal infection in the murine host (12–14, 36, 37), it is important to delineate the contribution of periplasmic flagella in all aspects of the natural infectious life cycle of *B. burgdorferi*.

In this communication, we intend to address two questions regarding the role of periplasmic flagella in *B. burgdorferi* morphology and persistence in relevant hosts. Recently, we reported that *flaB*-deficient (Δ*flaB*) cells lack the periplasmic flagellar filament and were nonmotile (14, 33). These results indicated that the periplasmic flagella are essential for the spirochete's flat-wave morphology (28). However, this does not distinguish whether motor rotation or the mere possession of periplasmic flagella is crucial for the flat-wave morphology; thus, we will directly address this issue both *in vitro* and *in vivo*. Second, the Δ*flaB* mutant cells failed to establish infection in C3H/HeN mice by either needle or tick transmission. Bacterial flagella are a potent immunogen and are agonists for Toll-like receptors (TLRs) (38, 39), and flagella have been the basis of vaccine candidates (40–42). Importantly, antibodies against the periplasmic flagellar filament are strongly detected in all stages of Lyme disease (43), and these *B. burgdorferi*-elicited antisera have been shown to be protective against subsequent infection (44), although the specific roles of endoflagellum-specific antibodies were not addressed. Interestingly, our preliminary observations of actively dividing *B. burgdorferi* in host tissues using intravital microscopy appear to show endoflagellar material exposed extracellularly for a brief period after dividing (R. M. Wooten, unpublished), suggesting such antibodies interact with intact spirochetes. To discriminate whether motor rotation and/or the possession of periplasmic flagella is necessary for disease production or migration within and between relevant hosts, we constructed a mutant of *motB* that retains the periplasmic flagella but whose cells are paralyzed. These studies demonstrate that motor rotation is crucial for the spirochete wave-like morphology and further delineate the importance of periplasmic flagellar motor rotation for spirochete survival in the tick, bacterial migration from the tick to the mouse, and infection of the mammalian host.

MATERIALS AND METHODS

Bacterial strains and growth conditions. A *B. burgdorferi* low-passage, virulent strain, B31-A3-K10, was used as the wild-type (WT) clone throughout the study (a kind gift from R. Rego and P. Rosa, Rocky Mountain Laboratories, NIH). This strain is a derivative of B31-A3 in which the *bbe002* gene located in linear plasmid 25 (lp25) was inactivated using a P_{flaB}-*aph1* (Kan^r) cassette to increase transformation frequency (45). Parental strain B31-A3 (and B31-A3-K10) retains all endogenous plasmids except circular plasmid 9 (cp9) (46). B31-A3 is a derivative of strain B31 that has been sequenced already (47). Construction of a *motB* mutant (Δ*motB*) and derivative strains are described below. Spirochetes were grown in Barbour-Stoenner-Kelly II (BSK-II) broth or semisolid plating BSK (PBSK) medium at 35°C in a humidified 2.5% CO_2 incubator (48).

Construction and complementation of *motB* mutant. The *motB* gene (locus *bb0280*, a 783-bp gene) is located in a large motility operon consisting of 26 flagellar genes (11, 47). The *motB* gene overlaps the upstream gene, *motA*, by 1 bp and is separated from the downstream *fliL* gene by 48 bp. The gene was inactivated by replacing the coding sequence of *motB* with the *aadA* coding sequence for streptomycin/spectinomycin resistance using overlapping PCR as described previously (49). The PCR product yielded a 2,905-bp product that was gel purified and cloned into the pGEM-T Easy vector (Promega Inc.) to yield the *motB*::*aadA*-pGEM plasmid. The integrity of the *motB* inactivation plasmid was confirmed by PCR and restriction mapping. The plasmid *motB*::*aadA*-pGEM was digested with NotI, and the purified linear DNA was electroporated into WT B31-A3-K10 competent cells. Electroporated cells were plated in semisolid PBSK medium containing 80 μg/ml streptomycin plus 200 μg/ml kanamycin (48). Resistant clones were analyzed by PCR as well as by Western blotting (see below) to confirm *motB* deletion.

The previously described shuttle vector pBSV2G (50), carrying a gentamicin resistance cassette (P_{flgB}-*aacC1*), was used to complement the *motB* mutant (Δ*motB*). The *B. burgdorferi flgB* promoter sequence (51, 52) and intact *motB* gene sequence were amplified separately with primers containing restriction enzyme sites XbaI and NdeI (5′-3′ and 3′-5′, respectively). The primers used were (5′-3′) the following: for the *flgB* promoter, FlgB-XbaI-F (TCTAGAGCCGGCTAATACCCGAGC) and FlgB-NdeI-R (CATATGGAAACCTCCCTCATTTAA), and for the *motB* gene, MotB.com-F (CATATGGCTTTGCGAATTAAGA) and MotB.com-R (TCTAGATTACTGCTTAATTTCCTT) (underlined sequences indicate restriction sites). PCR products were cloned separately into the pGEM-T Easy vector to yield plasmids P_{flgB}-Easy and pmotB-Easy, respectively. Both of the plasmids were digested with NdeI. The *motB* DNA released from pmotB-Easy was inserted into the NdeI site of the P_{flgB}-Easy vector, yielding the plasmid P_{flgB}-motB-Easy. This plasmid was digested with XbaI and then cloned into the same restriction site of the shuttle vector pBSV2G, yielding pmotB.com. Approximately 60 μg of purified pmotB-.com plasmid was used to transform competent Δ*motB* cells by electroporation as described above. Transformants were selected with 40 μg/ml gentamicin, 200 μg/ml kanamycin, and 80 μg/ml streptomycin. To confirm that the plasmid was complemented in *trans*, the pmotB.com shuttle vector was rescued from complemented *motB* (*motB*^{com}) *B. burgdorferi* cells, transformed, and then purified from *E. coli*. Purified, rescued vector was subjected to restriction digestion and DNA sequencing to confirm the integrity of the P_{flgB}-*motB* construct.

Gel electrophoresis and Western blot analysis. Sodium dodecyl sulfate-polyacrylamide gel electrophoresis (SDS-PAGE) and immunoblotting with an enhanced chemiluminescence detection method were carried out according to the manufacturer's instructions (GE Healthcare Co.). Exponentially growing *B. burgdorferi* cells were harvested and washed with phosphate-buffered saline (PBS) and resuspended in the same buffer. The protein concentration of cell lysates was determined using a Bradford protein assay kit (Bio-Rad Laboratories, Inc.). Approximately 5 μg of lysates was loaded into each lane of an SDS-PAGE and subjected to immunoblotting using specific antibodies. Monoclonal and polyclonal antibodies were generously provided by the following investigators: monoclonal anti-*B. burgdorferi* FlaB (H9724) by A. G. Barbour (University of California, Irvine, CA), monoclonal anti-*B. burgdorferi* DnaK by J. Benach (SUNY at Stony Brook, NY), polyclonal anti-*E. coli* FliM by D. Blair (University of Utah, Salt Lake City, UT), and polyclonal anti-*B. burgdorferi* MotB by J. Carroll (RML, NIH, Hamilton, MT). The reactivity of these antibodies to *B. burgdorferi* MotB, FliL, FliM, FlaB, and DnaK has been reported (14, 33, 49, 53, and our unpublished data).

Dark-field microscopy and swarm plate motility assays. *B. burgdorferi* cells (5×10^7 spirochetes/ml) were observed under a dark-field microscope (Zeiss Axio Imager M1), and images were captured using an AxioCam digital camera. Swarm plate motility assays were performed as described previously (14, 48). Approximately 10^6 bacteria in a 5-μl volume were inoculated into a 0.35% agarose plate containing PBSK medium diluted 1:10 in PBS. Since *B. burgdorferi* is a slow-growing organism (5- to

12-h generation time) (14), plates were incubated for 5 days at 35°C in a 2.5% CO_2 humidified incubator.

Statistical analysis. Statistical analyses were performed using an analysis of variance (ANOVA) test followed by a Tukey-Kramer multiple-comparison test to determine the significance between WT, mutant, and *motB*^{com} samples unless otherwise indicated. A *P* value of ≤0.05 between samples was considered significant.

Cryoelectron tomography (cryo-ET). *B. burgdorferi* cells were grown to late log phase (~8 × 10^7 cells/ml) as described above. Bacteria were centrifuged in 1.5-ml tubes at 5,000 × *g* for 5 min, and the pellets were resuspended in 40 μl PBS at a final concentration of ~2 × 10^9 cells/ml. After mixing with 15-nm gold clusters, 5 μl was deposited onto freshly glow-discharged holey carbon grids for 1 min. Grids were blotted with filter paper to remove excess fluid, followed by rapid freezing in liquid ethane maintained at −180°C using a gravity-driven plunger apparatus (22, 27). The resulting frozen-hydrated specimens were imaged at −170°C using a Polara G2 electron microscope (FEI Company) equipped with a field emission gun and a 4,000 by 4,000 charge-coupled device (CCD) (16-megapixel) camera (TVIPS Gmbh, Germany). The microscope was operated at 300 kV with a magnification of ×31,000, resulting in an effective pixel size of 5.7 Å. Using the FEI batch tomography program, low-dose single-axis tilt series were collected from each bacterium at a −8-μm defocus with a cumulative dose of ~100 $e^-/Å^2$ distributed over 65 images. Tilt angles were in the range of −64° and +64° with an angular increment of 2°. Tilt series were aligned and reconstructed using IMOD software (54).

3D visualization. Reconstructions of *B. burgdorferi* cells were segmented manually using the three-dimensional (3D) modeling software Amira (Visage Imaging). Three-dimensional segmentation of the flagellar filaments and outer and inner membranes was manually constructed (22, 24, 27).

Mouse infection studies. Mouse infection studies were performed as previously described (14, 55–57) using either C3H/HeN (Charles River Laboratories, Raleigh, NC) or C57BL/6 (National Cancer Institute) mice. These mouse strains possess similar susceptibilities to infection with *B. burgdorferi* and similar bacterial numbers in most tissues during persistent infection, although they can cause different levels of disease severity (58–60). For infectious dose studies, C3H/HeN mice were needle inoculated intradermally with either 3 × 10^3 or 5 × 10^6 of the indicated *B. burgdorferi* strains. Spirochetes were enumerated using a Petroff-Hausser chamber and verified by plating the cells and counting CFU (61). Three to four weeks postinoculation, mice were sacrificed and skin, bladder, and joint tissues were aseptically isolated and cultured in *B. burgdorferi* growth medium. Reisolation of *B. burgdorferi* from sacrificed mouse tissues was monitored for up to 35 days, and the presence of spirochetes in the growth medium was determined by dark-field microscopy. Sacrificed mouse tissues also were subjected to PCR analysis to detect *B. burgdorferi* DNA using *flaB* gene-specific primers (14).

For tick infection studies, naive *Ixodes scapularis* larvae were purchased from Oklahoma State University (Stillwater, OK). Larvae were artificially inoculated by immersion in exponential-phase (5 × 10^7 cells/ml) *B. burgdorferi* cells, as described previously (62). Approximately 200 immersed ticks were allowed to feed on each mouse for 5 to 7 days and then were collected after they dropped off the mice. Mice were sacrificed 3 weeks postrepletion, and the infectivity of each strain was assessed by reisolation of spirochetes from mouse tissues, as described above. A subset of larvae was dissected individually 7 days after repletion, and the isolated midguts were analyzed by immunofluorescence assay (see below) for the presence of spirochetes. A second set of fed larvae was analyzed by quantitative PCR (qPCR) at 7 days postrepletion to determine the spirochete load per tick, as described below.

DNA extraction and qPCR analysis of fed ticks. Ticks were crushed individually, and genomic DNA was extracted using a DNeasy blood and tissue kit according to the manufacturer's instructions (Qiagen Inc.). Individual tick DNA was analyzed by PCR to determine tick infectivity (spirochete positive) using *B. burgdorferi flaB* gene-specific primers. Spirochete burdens in the infected ticks were assessed by qPCR to quantify the *flaB* copy number, which was normalized to the tick *actin* gene (14).

Immunofluorescence assays (IFA). Ticks were dissected in 30 μl PBS–5 mM $MgCl_2$ on Teflon-coated microscopic slides, mixed by pipetting, and then air dried. To avoid quenching by hemin in the blood, dissected tick contents were 10-fold serially diluted (57, 62). Slides were blocked with 0.75% bovine serum albumin (BSA) in PBS containing 5 mM $MgCl_2$ for 30 min and then washed twice with PBS-5 mM $MgCl_2$. Spirochetes were detected using a 1:100 dilution of goat anti-*B. burgdorferi* antisera labeled with fluorescein isothiocyanate (Kirkegaard & Perry Laboratories, Inc.). Images were captured using a Zeiss Axio Imager M1 microscope connected to a digital camera.

Assessment of spirochete transmission to mice by encapsulated nymphs. Transmission of spirochetes to naive mice was assessed using freshly immersed nymphs. Naive nymphs were artificially infected by immersion with *B. burgdorferi* clones as described above. Mice were anesthetized, and groups of 10 to 30 nymphs were confined to capsules affixed to the shaved backs of naive mice (14, 63, 64). Ticks were allowed to feed until repletion (3 to 5 days). Fed and unfed (immersed) ticks were individually crushed on day 7 postrepletion to determine spirochete burden per tick using qPCR as described above. Mice were euthanized immediately after repletion, and the skin from the tick-bite site was extensively washed with sterile distilled water (dH_2O) to remove tick excreta. To reisolate or detect spirochetes from the sacrificed mice, a 2-cm by 2-cm section of skin encompassing the feeding site was excised and was cut into two portions for analyses. One portion of the skin was rinsed in 70% isopropanol and incubated in *B. burgdorferi* growth medium for up to 35 days. Joint and bladder tissues also were isolated from the sacrificed mice to assess whether the *B. burgdorferi* strains could disseminate from the infection site (i.e., negative controls). Additionally, the second portion of the tick-bite site skin and control skin (neck skin) from each mouse were processed for PCR to detect *B. burgdorferi* DNA using *flaB* gene-specific primers. These mouse- and tick-related protocols were approved by the East Carolina University Animal Care and Use Committee.

Intravital microscopy and quantitative measurement of *B. burgdorferi* in murine ear skin. C57BL/6 mice were housed in the Department of Laboratory Animal Medicine at the University of Toledo Health Sciences Campus. To visualize *B. burgdorferi* in live, intact mouse skin tissues, a wild-type clone, B31-A3, was transformed with a gentamicin-resistant (P_{flgB}-*aacC1*) suicide plasmid containing constitutively expressed *gfp* (P_{flaB}-*gfp*) flanked by the endogenous cp26 DNA as described previously (7). The insertion of P_{flaB}-*gfp* was within the *B. burgdorferi* plasmid cp26, and this clone is referred to as B31-A3-GFP or WT-GFP. The *motB* mutant plasmid (*motB*::*aadA*-pGEM), described above, was transformed into competent *B. burgdorferi* B31-A3-GFP cells in order to construct a *motB* mutant constitutively expressing green fluorescent protein (GFP) (Δ*motB*-GFP).

Spirochetes were enumerated by direct counting using a Petroff-Hausser chamber and dark-field microscopy and then resuspended so they contained the desired *B. burgdorferi* numbers in 10 μl BSK-II medium. Two days prior to injection, the outer ear surface of the mice was depilated (Nair) and the mice were allowed to rest. On the day of inoculation, mice were anesthetized by intraperitoneal injection of a standard restraint cocktail (ketamine, 65 to 75 mg/kg of body weight; xylazine, 6 to 8 mg/kg; and acepromazine, 1 to 2 mg/kg), followed by an intradermal injection of 10^6 WT-GFP or Δ*motB*-GFP spirochetes into an individual ear as a 10-μl bolus; the inoculum also contained 10^5 red fluorescent latex beads (1 μm; Sigma-Aldrich) to mark the injection site. For imaging, the anesthetized mouse was placed on a 37°C heated imaging stage to mount the tip of the ear with the dorsal side down. Imaging was performed using an Olympus FV1000 laser confocal microscope system with either a 20× or 40× dry lens or with a 63× water lens. Mice were imaged on the day of injection at high magnification, and digital zoom was used to capture detailed motility events, while later images at 3, 24, 48, and 96 h postin-

oculation were captured at ×40 to compare the number of spirochetes per viewing field.

At the indicated times postinoculation and after live imaging, the animals were euthanized and ear tissue samples were excised and flash frozen in liquid N_2. DNA then was extracted and qPCR performed using our published methods (65, 66). Briefly, ear tissues were sequentially incubated in collagenase A and proteinase A before recovering DNA by multiple phenol-chloroform extractions and ethanol precipitation, which was interspersed with digestion of RNA using DNase-free RNase. The DNA was quantified by absorbance at 260 nm, and working samples were diluted to 50 μg/ml for qPCR analyses using a Light Cycler 96 (Roche Diagnostics). Copy numbers for the mouse *nidogen* and *B. burgdorferi recA* genes present in each sample were calculated by extrapolation to standard curves using LightCycler software (Roche Diagnostics). The reported data represent *recA* values that were corrected by normalization based on the murine *nidogen* gene copy number. The primers (5′-3′) used to detect mouse *nidogen* were nido.F (CCA GCC ACA GAA TAC CAT CC) and nido.R (GGA CAT ACT CTG CTG CCA TC). The primers for *recA* were nTM17.F (GTC GAT CTA TTG TAT TAG ATG AGG CTC TCG) and nTM17.R (GCC AAA GTT CTG CAA CAT TAA CAC CTA AAG).

Coinfection studies. Groups of C57BL/6 mice were injected using the protocol described above for the intravital microscopy studies. Injections were performed intradermally into the ear skin using either 10^6 WT (B31-A3-K10) *B. burgdorferi*, 10^6 Δ*motB* mutant, or a combination of 5×10^5 of each strain (i.e., 10^6 total bacteria). Animals were sacrificed at the indicated times, and DNA was purified from the ear tissues as indicated above. qPCR analyses were performed as described above on the ear skin DNA to determine the relative amounts of WT and Δ*motB* mutant bacteria present in those tissues. The primer sets used (5′-3′) were the following: for *flaB* (detects both WT and Δ*motB* strains), *flaB*-FWD (TTG CTG ATC AAG CTC AAT ATA ACC A) and *flaB*-REV (TTG AGA CCC TGA AAG TGA TGC); for *motB* (detects WT only), *motB*-FWD (TGC GCA ATA AAC AAG CAT CTC), and *motB*-REV (CCT CTT TCT TCT TGC CTA ACT ACA); for *aadA* (streptomycin resistance gene; detects only Δ*motB* mutant bacteria), *aadA*-FWD (ATC ATT CCG TGG CGT TAT CC) and *aadA*-REV (GTC AGC AAG ATA GCC AGA TCA A). The reported data represent the values for the relevant *B. burgdorferi*-specific primer sets that were corrected by normalization based on the mouse *nidogen* gene copy number. To determine if there were differences in the ability of WT and Δ*motB* mutant bacteria, the competitive index (CI) was calculated as the mutant/WT ratio for output (i.e., bacterial levels in the skin) divided by the same ratio for input (67).

RESULTS

Inactivation of *motB* and complementation in *trans*. The *motB* gene is located in the middle of the *flgB* operon, which contains 26 flagellar genes and is transcribed by the housekeeping σ^{70} factor of RNA polymerase (Fig. 1A) (11, 52). In several species of bacteria, *motB* encodes a motor stator responsible for the generation of flagellar motor rotation; however, the role of this putative torque-generating unit in *B. burgdorferi* is unknown. To determine its role in *B. burgdorferi* motility, morphology, and the infectious life cycle, a *motB* mutant was constructed (Fig. 1A) using our recently developed gene inactivation methodology (49). PCR (not shown) and immunoblotting with a specific anti-MotB antibody (53) identified a 24-kDa protein band in wild-type (WT) cells which was not detected in the Δ*motB* mutant cells, indicating the successful construction of the mutant (Fig. 1B). *motB* is located in the middle of an operon; thus, inactivation of this gene may cause polar effects on downstream gene expression (Fig. 1A). Even though our gene inactivation methodology is reported not to impose any polar effects in *B. burgdorferi* or other spirochetes (24, 68), we performed immunoblot analyses to address this issue. Immunoblot analyses of WT and Δ*motB* cell lysates with specific antisera indicated that protein synthesis of downstream FliL or FliM was not affected in the Δ*motB* mutant (Fig. 1B), validating our previous reports (24, 49).

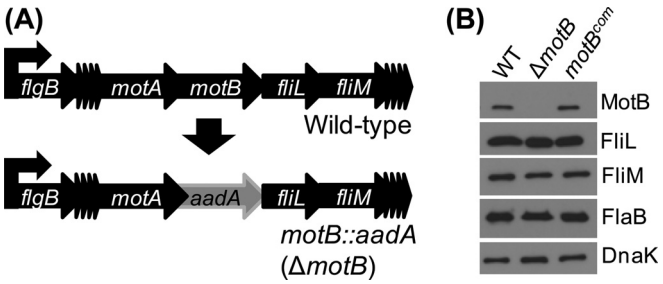

FIG 1 Inactivation and confirmation of *motB*::*aadA* (Δ*motB* mutant) strains. (A) Wild-type *B. burgdorferi flgB* operon contains 26 genes, including the target *motB* (top). The Δ*motB* genome was constructed by replacing the target gene with the streptomycin/spectinomycin resistance gene (*aadA*) (bottom). The complementation of Δ*motB* strain using the shuttle plasmid pBSV2G containing an intact *motB* gene transcribed by the *flgB* promoter is not shown. The model lists only a few of the 26 genes in the operon, and other genes are indicated by the multiple arrowheads. (B) Western blotting using polyclonal MotB-elicited antibody demonstrates the inhibition and restoration of MotB protein synthesis by the Δ*motB* and complemented $motB^{com}$ spirochetes, respectively. Potential Δ*motB* polar effects on the expression of downstream genes (*fliL* and *fliM*) were determined by FliL- and FliM-specific antisera, respectively. Flagellar synthesis was assessed using FlaB-specific antisera. DnaK was used as a loading control.

Even though the Δ*motB* mutant displayed no polar effects, the mutant was complemented in *trans* using the shuttle vector pBSV2G (50) containing an intact *motB* gene transcribed by the native *flgB* promoter. Restoration of MotB protein synthesis in the complemented *motB* ($motB^{com}$) cells was confirmed by immunoblotting (Fig. 1B). Finally, we verified that these strains retained all endogenous circular and linear plasmids that are present in the parental WT cells by PCR (45, 55, and data not shown); this also was supported by the ability of the *motB* mutant to have virulence restored by complementation in the subsequent *in vivo* assays (see below). Together, these results confirmed the construction of the Δ*motB* and $motB^{com}$ strains.

Morphology and motility phenotype of the Δ*motB* mutant. Since *motB* encodes the motor stator, a mutation in a functional *motB* gene should result in paralyzed bacteria (69, 70). To determine the *B. burgdorferi* Δ*motB* mutant motility phenotype, these strains were analyzed *in vitro* using dark-field microscopy and swarm plate motility assays. Dark-field microscopy indicated that the mutant cells were completely nonmotile, while the WT and the complemented cells were motile. Swarm plate assays indicated that the WT and complemented $motB^{com}$ cells possess similar swarming motility, but the Δ*motB* cells were unable to migrate from the initial site of inoculation and produced significantly less swarm ($P < 0.001$) than their parental WT or $motB^{com}$ cells (Fig. 2, bottom). To ensure that the paralyzed phenotype is not due to a lack of FlaB production (14, 33, 71), immunoblot analyses were performed using FlaB-specific antibodies (Fig. 1B, FlaB blot). Δ*motB* cells did synthesize FlaB but were nonmotile, suggesting that the Δ*motB* strain lacked the torque-generation properties associated with MotB. Additionally, Δ*motB* cells largely exhibited a wave-like morphology similar to that of WT cells; however, the middle portion of the Δ*motB* cells had an irregular rod-shaped morphology despite synthesizing similar levels of FlaB (Fig. 2,

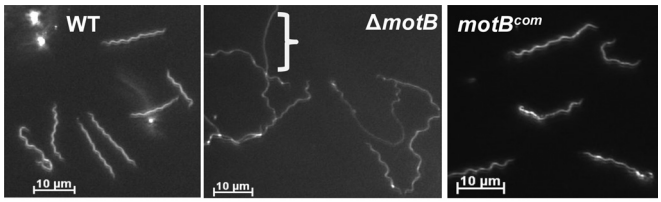

Strain	Swarm diameter (mm)
WT	16 ± 0.5
Δ*motB*	7.5 ± 0.5*
motB^{com}	15.7 ± 0.9

FIG 2 Morphology and motility phenotype of the Δ*motB* strain *in vitro*. (Top) Morphology of the *B. burgdorferi* strains was determined using dark-field microscopy. The bracket indicates a rod-shaped area in a Δ*motB* cell; several other areas also are visible. (Bottom) The indicated *B. burgdorferi* strains were inoculated into 0.35% soft-agarose plates, and their swarming was measured after 5 days. Values are indicative of the averages from at least 3 plates per strain. An asterisk indicates values that are significantly different from those for WT or complemented *motB*^{com} *B. burgdorferi* ($P < 0.001$), as determined by ANOVA test followed by Tukey-Kramer multiple-comparison test.

top). Complementation of the Δ*motB* mutant restored the normal flat-wave morphology and motility phenotypes (Fig. 2). Together, these results indicated that the lack of both motility and normal morphology that the Δ*motB* strain exhibited was due solely to the mutation in *motB* and not a secondary mutation elsewhere. MotA and MotB together form the stator complex; thus, a mutation in *motB* may interfere with the synthesis of MotA and/or assembly of a functional stator complex. However, the fact that the Δ*motB* mutant was readily complemented, and both *in vitro* and *in vivo* phenotypes were restored in the complemented *motB*^{com} cells (see below), indicate that MotA synthesis occurred at nearly normal levels.

Periplasmic flagellar motor rotation is crucial for *B. burgdorferi* flat-wave morphology. To more directly address any physical deficiencies that cause the irregular morphology displayed by the Δ*motB* mutant, cryoelectron tomography (cryo-ET) was performed to visualize the periplasmic flagella in intact spirochetes (24, 27, 49). For WT *B. burgdorferi*, 7 to 11 periplasmic flagella are inserted near each pole of the cell and extend toward the middle of the bacteria, resulting in a structured wrap around the cell body (11, 30). Cryo-ET data indicated that the periplasmic flagellar filaments of the WT and the *motB*^{com} cells formed a compact ribbon-like structure (Fig. 3, top left and bottom right), as

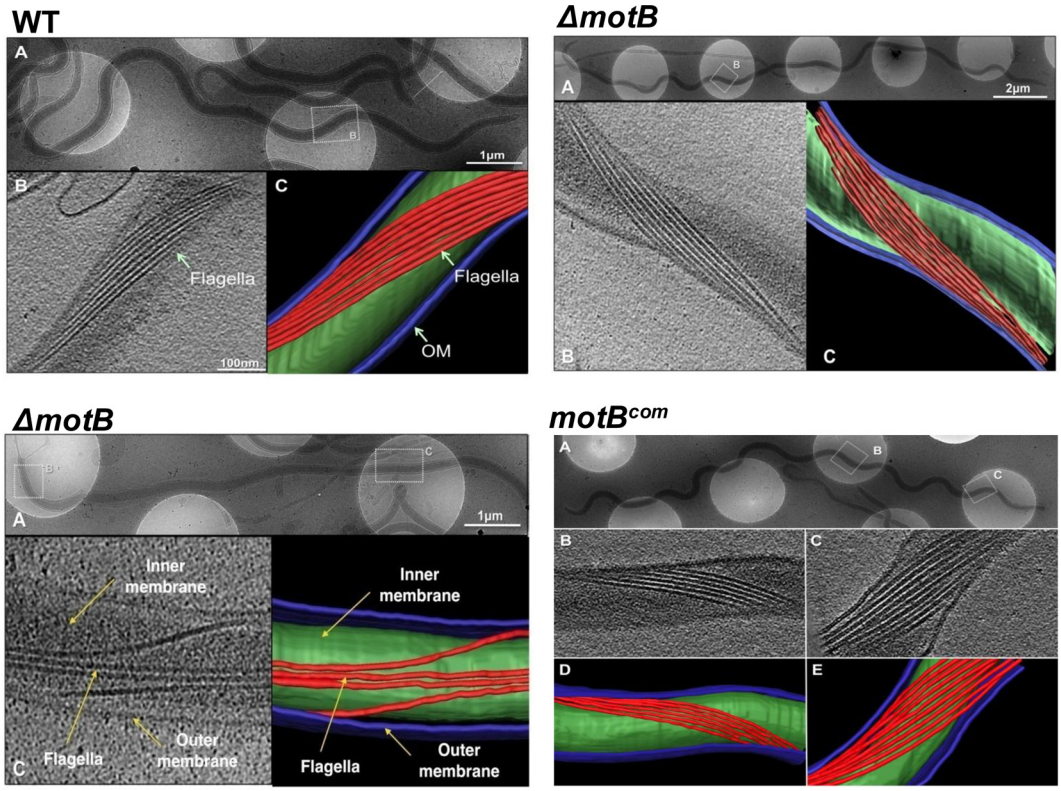

FIG 3 Assessment of the flagellar ribbon formation in *B. burgdorferi*. The indicated *B. burgdorferi* strains were grown *in vitro* and subjected to cryo-ET. (Top left set of images) Native cellular structures of WT *B. burgdorferi*. (A) Representative flat-wave cell morphology of a WT cell is shown in a low-magnification picture. (B and C) A representative tomogram of a local region (boxed) shows the periplasmic flagellar ribbon. Shown are one slice from a 3D tomogram (B) and a 3D surface rendering of the tomogram (C). The outer membrane (OM) is colored blue, the inner membrane is colored green, and periplasmic flagellar filaments are colored red. (Top right) Cell morphology and flagellar ribbon of a representative Δ*motB* cell. (A) The Δ*motB* cell exhibits regular flat-wave morphology near the cell pole. A cryo-ET section (B) and surface rendering (C) of the boxed region in panel A shows a normal flagellar ribbon. (Bottom left set of images) (A) Irregular, rod-shaped morphology of a Δ*motB* organism is shown (middle portion of the cell). A cryo-ET section from the rod-shaped region (B) and 3D surface rendering of the tomogram (C) show that the periplasmic flagellar ribbon is not ordered in those regions boxed in panel A. (Bottom right set of images) (A) Cell morphology and periplasmic flagellar ribbons of the *motB*^{com} spirochete. Tomograms from two different regions (B and C) show that the periplasmic flagellar ribbons are restored to normal flat-wave morphology. (D) Surface rendering is segmented from the tomogram shown in panel B. (E) 3D surface rendering resulting from the tomogram.

TABLE 1 Δ*motB* strain infectivity in mice via needle inoculation[a]

Strain	Dose[b]	Reisolation from tissues (no. of specimens positive/total no. examined)			No. of infected mice/total no. challenged
		Ear	Bladder	Joint	
WT	3×10^3	2/4	4/4	4/4	4/4
Δ*motB*	5×10^3	0/4	0/4	0/4	0/4
Δ*motB*	3.75×10^6	0/4	0/4	0/4	0/4
motB^{com}	3.4×10^3	3/4	4/4	4/4	4/4

[a] C3H/HeN mice were injected intradermally using the indicated *in vitro*-grown spirochete clones. Mice were sacrificed 3 weeks postinoculation, and infectivity was determined by reisolation or detection of *B. burgdorferi* genomes by PCR from sacrificed mouse tissue samples.

[b] The number of spirochetes injected per mouse was calculated by direct counting of bacteria using a Petroff-Hausser chamber. The calculated inocula were plated to verify the CFU, and doses shown are the actual CFU injected per mouse.

reported previously (32). While this ordered ribbon also was visible in the Δ*motB* mutant wave-like regions (top right) and the bacterial poles, the ribbon became distorted in the central rod-shaped areas of the Δ*motB* mutant (Fig. 3, bottom left). These data suggest that rotation of the flagellar motor is crucial for the appropriate ribbon formation by the periplasmic flagella to produce the spirochete's characteristic flat-wave morphology.

Δ*motB* cells are unable to establish murine infection by needle inoculation. To determine if the paralyzed but flagellated Δ*motB* cells are able to infect mice, 3×10^3 or 3×10^6 *in vitro*-grown WT, Δ*motB*, or *motB*^{com} spirochetes were intradermally inoculated into groups of C3H/HeN mice. Three weeks postinoculation, mice were sacrificed and bacterial persistence was determined by the outgrowth of spirochetes from the collected mouse tissues. While WT and *motB*^{com} spirochetes were detected in two or more tissues assessed from all mice infected with the lowest dose (3×10^3), no positive tissues were identified in mice inoculated with the Δ*motB* mutant spirochetes, even at the highest dose (3.75×10^6) (Table 1). Furthermore, no tissues from Δ*motB* mutant-inoculated mice (joint and ear skin) were positive for *B. burgdorferi* DNA by PCR analysis using *flaB*-specific primers (not shown), indicating that MotB is required for infection of mice.

Infection kinetics initially were assessed by intradermal injection of wild-type and Δ*motB* strains engineered to constitutively express GFP into murine ear skin and subsequent visualization within the intact skin of the live mice using laser confocal microscopy. At 6 h postinjection, many WT-GFP bacteria were observed displaying characteristic spirochetal morphology and motility, whereas the majority of Δ*motB*-GFP cells appeared in clumps. Notably, Δ*motB*-GFP cells were completely nonmotile and displayed no spirochetal morphology, even at the two poles as detected in these mutants *in vitro* (see Fig. S1 in the supplemental material). Within 2 to 3 h postinjection, a substantial number of WT-GFP cells were observed migrating away from the central injection site (see red beads in Fig. S2), while a diminished number of mutant Δ*motB*-GFP cells remained entangled at the injection site and displayed no motility (see Fig. S2). However, after a few days of cell numbers remaining stable, the highly motile WT-GFP cell numbers began to increase and were observed to have migrated a substantial distance from the injection site (see Fig. S2). However, the Δ*motB*-GFP cells appeared to be largely cleared from the tissues by 24 to 48 h postinoculation.

To more definitively quantify the observed clearance, parallel groups of mice were injected with either the WT-GFP or Δ*motB*-GFP cells, and the entire ear tissues were harvested at different times postinjection for qPCR analyses to determine spirochete numbers. At 30 min postinjection, similar numbers of WT-GFP and Δ*motB*-GFP genomes were detected, confirming that equal inocula were delivered (Fig. 4). While both strains showed a substantial decrease by 24 h, the WT-GFP numbers remained stable and were observed to increase significantly after 48 h postinjection, similar to our previous reports (66). Conversely, the Δ*motB*-GFP numbers were barely detectable by 24 h, and no mutant bacteria were detected ≥48 h postinfection (Fig. 4). Together, these findings indicate that Δ*motB*-GFP cells are completely nonmotile *in vivo* and are cleared by the host immune defenses within 24 to 48 h postinoculation. These findings also are supported by enzyme-linked immunosorbent assay (ELISA) analyses showing that only barely detectable levels of *B. burgdorferi*-specific IgG were elicited in response to Δ*motB* mutant infection (data not shown).

Δ*motB* spirochetes cannot infect mice via tick transmission. Although naive mice were not infected by needle injections, it is possible that the Δ*motB* spirochetes could establish infection in mice via tick bite, as arthropod-derived wild-type *B. burgdorferi* were reported to show enhanced infectivity compared to that of needle-introduced spirochetes (72, 73). Accordingly, *Ixodes scapularis* larvae were artificially inoculated using immersion with exponentially (5×10^7 cells/ml) growing WT, Δ*motB*, or *motB*^{com} spirochetes and subsequently allowed to feed on C3H/HeN mice. Bacterial outgrowth analyses determined that no murine tissues harvested at 3 weeks postinfection contained Δ*motB* spirochetes, whereas all mice fed with WT- and *motB*^{com} mutant-immersed ticks showed bacterial growth (Table 2). A subset of fed ticks was crushed individually 7 days after the blood meal, and immunofluorescence assays (IFA) were performed in order to detect spirochetes in the midguts. IFA results indicated that all three strains could be detected in the midguts (see Fig. S3 in the supplemental material). Finally, another subset of fed larvae was processed similarly to isolate DNA for qPCR assessment of spirochetal loads per fed tick. Notably, the Δ*motB* spirochete load per fed larva was significantly lower ($P < 0.05$ or $P < 0.001$) than that for the ticks

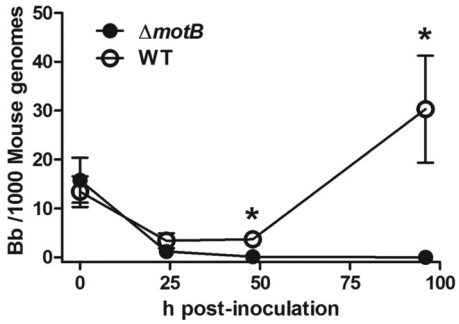

FIG 4 Clearance kinetics of WT-GFP and Δ*motB*-GFP bacteria from murine skin. A total of 10^6 WT-GFP (wild-type) or Δ*motB*-GFP (Δ*motB* mutant) bacteria were injected intradermally into murine ear skin. Entire ear tissues were collected at the indicated times postinjection, and tissue DNA was enumerated for *B. burgdorferi* (Bb) content by qPCR. Each circle represents the average value ± standard error of the mean (SEM) (error bar) from at least four separate ears assessed at each time point. *, $P < 0.004$ by Mann-Whitney U test.

TABLE 2 Δ*motB* strain infectivity in mice via feeding of immersion-infected larval ticks[a]

B. burgdorferi clone in larval ticks	Reisolation from tissues (specimens positive/total no. examined)			No. of mice infected/no. of mice tested[b]
	Ear	Bladder	Joint	
WT	5/7	7/7	7/7	7/7
Δ*motB*	0/9	0/9	0/9	0/9
motB^{com}	8/9	9/9	9/9	9/9

[a] Larval ticks were artificially infected by immersion with exponentially growing bacteria (5×10^7 cells per ml). Approximately 200 immersed larvae were fed per C3H/HeN mouse. Mice were sacrificed 3 weeks postrepletion.
[b] Infectivity was determined by reisolation of *B. burgdorferi* from sacrificed mouse tissue samples. Data represent two independent studies with different batches of ticks.

TABLE 3 Persistence of Δ*motB* mutant spirochetes in nymphal ticks before and after a blood meal[a]

Nymph artificially infected with *B. burgdorferi* clone	No. of spirochete-infected nymphs/total no. tested (% positive)	
	Unfed	Fed
WT	15/15 (100)	15/15 (100)
Δ*motB*	15/15 (100)	3/35 (8.6)
motB^{com}	14/15 (93)	15/15 (100)

[a] Unfed and fed nymphs infected by immersion were squashed individually on day 7 postrepletion for DNA isolation. Infection efficiency of the ticks by *B. burgdorferi* (% positive) was determined by *flaB* gene-specific PCR. A representative result from two independent assays is shown.

containing the WT or *motB*^{com} bacteria (Fig. 5). Together, these results indicate that mice are not able to be infected with the Δ*motB* strain by larval tick bite and that either periplasmic flagella or motility is crucial for optimal survival of spirochetes in fed ticks.

Evaluation of Δ*motB* strain viability in nymphal ticks and transmission from nymphs to mice. The studies described above suggest that Δ*motB* spirochetes were not infectious in mice either because they failed to migrate out of the tick during feeding or because the mutant spirochetes were able to transmit from tick to mice but subsequently were cleared from the mouse skin by host immune responses. Moreover, we were unsure if the larvae that were artificially infected (by immersion) with the mutant cells had a spirochete burden equal to that of the parental or *motB*^{com}-infected ticks, even though we immersed the ticks in the same density of spirochetes. Since the size of an immersed but unfed larval tick is quite small (less than 1 mm), it is not technically feasible to collect sufficient *B. burgdorferi* DNA from an individual larvae to determine spirochete genomes. Alternatively, collection of DNA from a batch of unfed larvae can lead to inaccurate results (our unpublished observation). To address all of these issues, naive

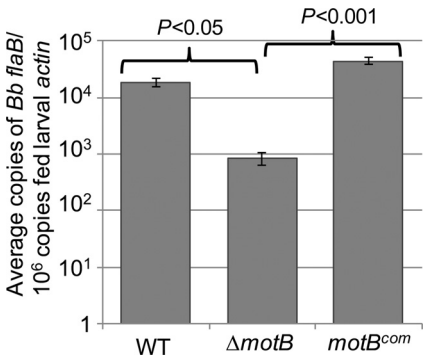

FIG 5 Persistence of Δ*motB* cells in fed larval ticks. Quantitative PCR analysis of the *B. burgdorferi* load in individual fed larvae that were collected 7 days after repletion. Spirochete numbers were quantified using *flaB* primers and are normalized to tick *actin* gene levels. A representative result from two independent studies with different batches of ticks is shown here. Bars represent the mean *flaB* values per larva ± standard errors of the means (SEM) for each isolate (4 spirochete-positive ticks per strain per assay). *P* values for Δ*motB* strain-infected ticks were significantly lower than that for the corresponding WT ($P < 0.05$) or isogenic complemented *motB*^{com} ($P < 0.001$) strain. Statistical analysis was performed using an ANOVA test followed by Tukey-Kramer multiple-comparison test.

nymphs were artificially infected by immersion before they were encapsulated onto naive C3H/HeN mice. Artificially infected unfed and fed nymphs were squashed individually 7 days postrepletion, followed by *flaB* gene-specific PCR to determine the percentage of spirochete-positive ticks. Before feeding on naive mice, 100% of the nymphs were positive for both WT and mutant spirochetes (Table 3, unfed nymphs). In contrast, the infection rate of Δ*motB* mutant-infected ticks was markedly decreased to 9% after feeding, while this rate remained unchanged for the WT or the complemented *motB*^{com} cells (Table 3, fed nymphs). qPCR assessment of the spirochete burden within the PCR-positive ticks indicated the Δ*motB* spirochete levels were similar or higher in unfed ticks, indicating the immersed nymphs were infected equally by all three *B. burgdorferi* strains (Fig. 6A). However, at 7 days postfeeding, the Δ*motB* spirochete burden in ticks was significantly lower than that of WT ($P < 0.01$) or *motB*^{com} ($P < 0.001$) cells (Fig. 6B). Immediately after tick feeding, multiple mouse tissues were collected and processed to determine *B. burgdorferi* transmission by using outgrowth and PCR analyses. PCR of DNA isolated from the tick-bite site skin tissues indicated that the Δ*motB* genomes were not detectable using *flaB* or *enolase* gene-specific primers, while the parental or isogenic complemented *motB*^{com} bacteria were readily detected. Similar results were obtained by the bacterial outgrowth protocol (Table 4). Together, these results indicate that motility is crucial for the persistence of spirochetes in fed ticks as well as transmission to and infection of mice.

Δ*motB* bacteria display decreased growth rate *in vitro*. The studies described above indicated that the viability of Δ*motB* spirochetes in fed but not unfed ticks was significantly less than that for the parental *B. burgdorferi*-infected ticks. One possibility is that the flagellated, nonmotile Δ*motB* mutant grows at a lower rate *in vitro* than the WT, which may contribute to the lower spirochete burden *in vivo* (in ticks after, but not before, feeding on mice). To investigate this, the *B. burgdorferi* strains were cultured *in vitro* and enumerated using a Petroff-Hausser counter daily for 7 to 8 days or until the cells reached stationary phase (1×10^8 to 2×10^8 cells per ml). As shown in Fig. 7, the growth rate of the Δ*motB* mutant is significantly lower than that of the WT or complemented *motB*^{com} cells, suggesting a growth defect *in vitro* ($P = 0.01$).

Coinfection with Δ*motB* mutant and wild-type *B. burgdorferi* has no effect on survival of either strain *in vivo*. Since motility appears to be essential for evasion of host immune clearance, we performed coinfection studies to address whether the characteristic motility exhibited by WT *B. burgdorferi* affects the clearance of the Δ*motB* strain and perhaps enhances evasion of host

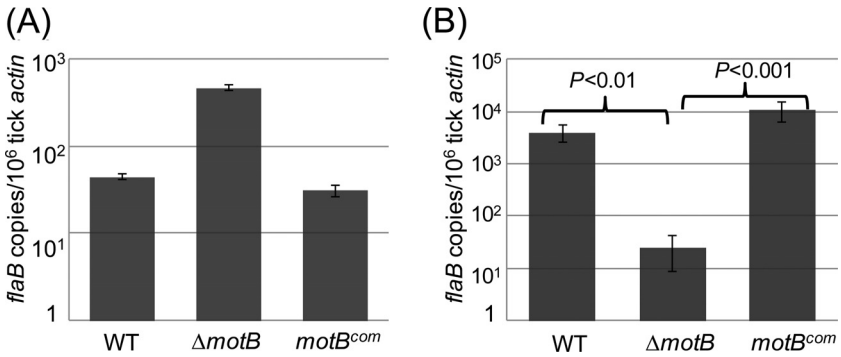

FIG 6 Viability of Δ*motB* cells in fed and unfed nymphs. Naive nymphal ticks were artificially infected using *in vitro*-grown spirochetes. Unfed (A) and fed (B) nymphs were crushed individually on day 7 postrepletion, and the spirochetal load per nymph was determined by qPCR using only the DNA from the PCR-positive ticks. Results shown are means ± SEM from 3 positive ticks per strain. Data are representative of two independent studies. *P* values were determined by Kruskal-Wallis test followed by Dunn's multiple-comparison test.

clearance. WT and Δ*motB* mutant cells were needle injected intradermally into murine ear skin as a single strain or as a mixture (1:1 ratio), and these tissues were harvested for DNA purification and qPCR analysis at different times postinjection. Analyses using a *flaB* primer set that detects both strains indicated that similar doses of bacteria were inoculated into the ear skin at 6 h postinjection for both single-strain and coinfection groups (Fig. 8A). By 48 h, all inoculation groups were significantly reduced compared to levels at 6 h, indicating substantial immune clearance of both strains. However, at 96 h the mice injected only with the WT displayed significant proliferation in tissues, whereas the mice inoculated only with the Δ*motB* mutant contained no spirochetes. Mice receiving the mixture displayed approximately 50% of the bacterial numbers contained by the WT-infected mice, suggesting that the surviving spirochetes represented the outgrowth of WT only. Analyses using a *motB* primer set that detects only *B. burgdorferi* containing the intact *motB* (i.e., WT) displayed the same survival trend as the *flaB* analyses, again suggesting that only the WT bacteria were surviving (Fig. 8B). A third analysis using an *aadA* primer set that only recognizes spirochetes containing the streptomycin resistance gene (i.e., Δ*motB*) confirmed the accuracy of the initial coinfection inoculum and that all of the spirochetes detected at 96 h postinfection represented WT bacteria (Fig. 8C). Calculation of the competitive index indicated that, while no significant differences were noted at 48 h, the Δ*motB* mutant was much less fit than WT *B. burgdorferi* at 96 h postinfection (Fig. 8D). Together, these findings indicate that the spirochetal motility displayed by WT *B. burgdorferi* had no effect on the ability of the host immune system to clear the nonmotile Δ*motB* mutant and vice versa.

TABLE 4 Transmission of Δ*motB* mutant spirochetes from freshly infected nymphs to mice

B. burgdorferi clone used to infect nymphs[a]	No. of mice infected/total no. of mice tested
WT	5/6
Δ*motB*	0/6
motB^{com}	6/6

[a] Ten nymphs immersed in WT or *motB*^{com} mutant spirochetes and 30 nymphs immersed in Δ*motB* mutant spirochetes were allowed to feed per C3H/HeN mouse using the capsule method. Immediately after most ticks dropped off, mice were sacrificed. Two sections of skin tissue from the tick bite site were assessed for the presence of *B. burgdorferi* by regrowth in culture medium and detection of *B. burgdorferi* genomes using *flaB-enolase* gene-specific PCR.

DISCUSSION

In many motile bacteria, MotA and MotB together form a torque-generating unit powered by a proton motive force. Thus, a mutation in *motA* or *motB* produces bacteria that are flagellated but paralyzed. Furthermore, bacterial shape typically is not altered by a mutation in these genes (20, 70, 74). Although *B. burgdorferi* motor proteins share significant amino acid sequence homology with other bacteria, a *motA* or *motB* mutant has not been reported in any spirochete. Thus, the effect of motor rotation on periplasmic flagellar organization, cellular morphology, and infectivity/persistence was unknown. Using cryo-ET and intravital microscopy images of the *B. burgdorferi* Δ*motB* mutant, it was revealed for the first time that, while the possession of periplasmic flagella is essential for forming the normal flagellar ribbon structure, motor rotation is required to form the highly organized ribbon that produces the characteristic flat-wave morphology exhibited by this spirochetal bacterium. Bacterial cell cylinders and flagella are thought to be elastic materials (11, 28). Thus, applied forces cause these structures to deform and subsequently revert back to their

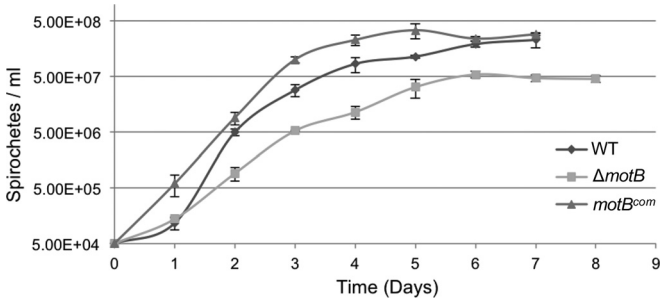

FIG 7 *In vitro* growth curves of WT, Δ*motB*, and complemented *motB*^{com} *B. burgdorferi* strains. The indicated *B. burgdorferi* strains were inoculated into BSK-II medium (5×10^4 bacteria/ml), incubated at 35°C, and counted at the indicated times by direct enumeration using a Petroff-Hausser chamber. Cell density at each time point is indicated as the mean ± standard deviation from three independent cultures (triplicates of each culture per strain). The growth rate of the Δ*motB* mutant strain was significantly reduced ($P = 0.01$; paired Student's *t* test) compared to that of the parent or *motB*^{com} strain during days 2 to 7.

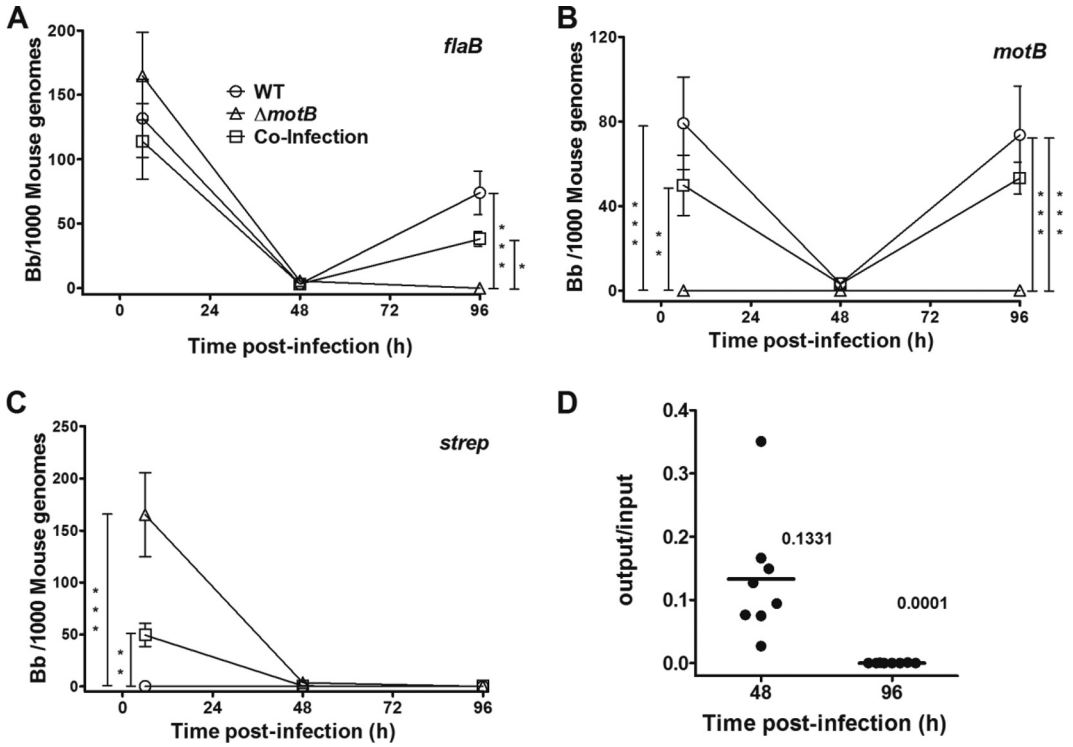

FIG 8 Effects of coinfection on the *in vivo* clearance of WT and Δ*motB B. burgdorferi* strains. A total of 10^6 WT (open circle), Δ*motB* (open triangle), or both (5×10^5 each strain; open square) strains were injected intradermally into murine ear skin, and the bacterial numbers were enumerated at the indicated times postinoculation by qPCR using three different primer sets: *flaB* detects both strains (A), *motB* detects WT only (B), and *strep* detects the streptomycin resistance gene present only in the Δ*motB* strain (C). Each symbol represents the average and standard error from at least 8 separate ear tissue samples. *, $P < 0.05$; **, $P < 0.01$; ***, $P < 0.001$ by Kruskal-Wallis test followed by Dunn's multiple-comparison test. (D) Competitive index (CI) is the ratio of Δ*motB* mutant to WT bacteria detected at that time point (output) divided by the same ratio for the inoculum that was initially injected (input). The short horizontal lines represent the average values.

original shape when the force is removed. Several studies have demonstrated that the *B. burgdorferi* cell cylinder is rod shaped in the absence of periplasmic flagella, whereas purified periplasmic flagella are shown to be helical. Thus, the interaction between the cylinder and flagella produces the distinct spirochetal flat-wave morphology (11, 28, 32). Based on these findings, we predict that the flagellar ribbon interacts with the cell cylinder, and this physical interaction is enhanced by forces provided by flagellar rotation to produce the ordered ribbon structure, which in turn produce the spirochete's wave-like morphology. Conversely, spirochetal cells that exhibit any motility by rotating their motors also should display flat-wave morphology (e.g., Δ*cheA2*, Δ*cheY3*, Δ*fliG1*, and Δ*cheX* strains) (12, 29, 75, 76). In the absence of this rotation force, it appears that the ribbon structure is not maintained throughout the cell cylinder, particularly in those midsection areas where the two opposite flagellar ribbons overlap, resulting in disordered flagellar bundles and a more rod-like morphology in those regions.

Although the Δ*motB* bacteria failed to establish infection in mice, this result was not completely surprising given the fact that other reported nonmotile, aflagellated, or reduced-motility mutants in several spirochete species are attenuated in their respective host (12, 14, 36, 77–80). However, flagellin molecules are recognized by Toll-like receptor 5 (TLR5) and TLR11 in mice, which can activate host inflammatory responses (81, 82). Additionally, bacterial flagella are a potent immunogen and elicit adaptive immune responses, which has formed the basis for several vaccine strategies (41, 42). Thus, it was unknown how the lack of the agonistic/immunogenic properties possessed by bacterial flagella (i.e., Δ*flaB* [14]) influenced the persistence in host tissues versus *B. burgdorferi* strains that possess periplasmic flagella but are unable to generate the torque required for spirochetal motility (i.e., Δ*motB*). Our results with the flagellated but nonmotile Δ*motB* mutant indicated that these bacteria also were unable to infect mice by needle inoculation (Table 1 and Fig. 4), similar to the Δ*flaB* strain (14). This phenotype also is similar to that for *S.* Typhimurium and *Helicobacter* flagellated nonmotile mutants that were less efficient than the parental cells or completely lost the ability to colonize their respective host (83–87). Since several pathogenic nonmotile aflagellated mutants, including the spirochetes, are severely attenuated or not able to colonize their animal hosts, we propose that spirochetal motility is crucial for evasion of immune clearance by mammalian hosts and is independent of any immune-associated properties related to the flagellar proteins. The requirement of bacterial motility to establish infection ranges from vital to expendable in different bacterial species (86, 88–91). Since the flagella of spirochetes are periplasmic and *B. burgdorferi* is an invasive organism that can travel through dense tissues (9), we propose that the torque provided by MotB activities enable the flagellar motility that is crucial for mediating bacterial dissemination, evasion of the cellular immune responses, and eventual colonization of multiple distant tissues to elicit Lyme disease. Our

data support this, since the nonmotile Δ*motB* bacteria are cleared by the host immune responses within 48 h of inoculation into murine skin (Fig. 4; also see Fig. S1 and S2 in the supplemental material), which is substantially earlier than when *B. burgdorferi*-specific antibodies normally are expressed in infected mice (92). However, further studies using mouse strains deficient in different innate and adaptive immune cells and/or mediators are required to completely define which are evaded due to spirochetal motility.

In nature, mammalian hosts become infected via *B. burgdorferi*-infected tick bite (3, 4). Accordingly, we performed tick-mouse infection assays to determine the importance of MotB in spirochetal transmission from the tick to the mouse and for their ability to survive in the tick. In these months-long protocols, we demonstrated that flagellar motor rotation (i.e., motility) was crucial for migration of spirochetes from the tick to the mouse (Tables 2 and 4). Because no Δ*motB* mutant spirochetes were observed by reisolation or PCR from any tick-bite site (or from other mouse tissue samples), it appears that the Δ*motB* strain cannot be transmitted into the mouse via tick bite (Tables 2 and 4). This result was not surprising, since the tick midgut epithelial cells possess tight junctions that likely require the great force provided by the back-and-forth spirochetal motility to traverse this barrier and subsequently be deposited into skin (7). This is in agreement with findings that certain spirochete mutants that lack motility, the run-and-reverse type of motility, or fail to reverse (e.g., Δ*flaB* and Δ*cheA2* mutants) also were unable to migrate out of the tick vectors (13, 14). Together, our data strongly support that motility is a prominent factor for bacterial dissemination within and between hosts.

When spirochete viability in fed ticks was assessed in greater detail, optimal viability was observed only in the WT and complemented strains (Table 3 and Fig. 5 and 6). The lower Δ*motB* spirochete burden in the fed ticks could reflect the reduced growth rate observed for Δ*motB* spirochetes *in vitro* (Fig. 7), although no studies could be devised to confirm whether a similar growth defect occurs *in vivo* (i.e., in ticks). Another possibility is that fewer Δ*motB* bacteria were ingested during tick immersion than were the motile strains, but the studies outlined in Fig. 6A indicate that all strains were similarly ingested by the nymphs. Thus, the most likely explanation for the reduced burden is that Δ*motB* cells are unable to replicate at the same rate as the motile strains within ticks, or they were more efficiently cleared from the fed tick midgut by host blood components, blood-induced tick factors present in the midgut, or the tick immune system (93–95). It is notable that these nonmotile mutants often grow *in vitro* as knots of cells that appear to be unable to completely separate from the mother cell, suggesting that motility is important for efficient separation of replicating cells, both in liquid media and in host tissues (data not shown) (14, 96).

Surprisingly, we discovered that the mutant bacteria failed to effectively survive in ticks for ≥7 days after the blood meal (Table 3 and Fig. 6B). Even if the Δ*motB* bacterial burden per tick was significantly lower due to an *in vivo* growth defect, the rate/percentage of the spirochete-positive ticks would be expected to remain unchanged after the blood meal. However, that did not happen. As shown in Table 3, the percentage of mutant-infected ticks dropped sharply from 100% to 9%, while this rate remained unchanged with the nymphs colonized with WT or the *motB*^{com} spirochetes. These results led us to predict that WT motility promotes an intimate bacterial interaction in the tick midgut (e.g., *B. burgdorferi* outer surface protein OspA with tick midgut protein TROSPA), and this interaction protects the organism from potential harm from the blood-induced factors or tick immune responses (94, 97). Alternatively, the Δ*motB* organisms may have failed to acquire nutrients in the midgut due to their lack of motility; thus, they are less likely to survive after the blood meal. These conclusions are supported by studies where spirochetes that exhibit even limited modes of motility, including running in one direction (Δ*cheA2* and Δ*pdeA* Δ*bb0363* mutants) or only the flex type of motility (Δ*cheX* mutant), are able to survive normally in fed ticks (13, 57, and our unpublished data). Altogether, our studies indicate that possession of flagella is essential for motility and infectivity (14), but without the additional machinery that allows periplasmic flagellar rotation (e.g., MotB), the flagellum itself provides no additional properties to enhance spirochetal infectivity or evasion of host immune clearance.

ACKNOWLEDGMENTS

We thank P. Rosa, R. Rego, A. Barbour, J. Benach, M. Caimano, J. Carroll, and D. Blair for sharing reagents. We also thank E. Novak for critical reading of the manuscript and N. Charon for helpful discussion.

This research was supported by the National Institute of Arthritis, Musculoskeletal, and Skin Diseases, NIH (AR060834 to M.A.M. and R.M.W.), the National Institute of Allergy and Infectious Disease (R01AI087946 to J.L. and M.A.M.), the American Heart Association (predoctoral fellowship to P.S.), and the Welch Foundation (AU-1714 to J.L.).

REFERENCES

1. **Kurtenbach K, Hanincova K, Tsao JI, Margos G, Fish D, Ogden NH.** 2006. Fundamental processes in the evolutionary ecology of Lyme borreliosis. Nat Rev Microbiol **4:**660–669. http://dx.doi.org/10.1038/nrmicro1475.
2. **Lane RS, Piesman J, Burgdorfer W.** 1991. Lyme borreliosis: relation of its causitive agent to its vectors and hosts in North America and Europe. Annu Rev Entomol **36:**587–609. http://dx.doi.org/10.1146/annurev.en.36.010191.003103.
3. **Brisson D, Drecktrah D, Eggers CH, Samuels DS.** 2012. Genetics of *Borrelia burgdorferi*. Annu Rev Genet **416:**513–534. http://dx.doi.org/10.1146/annurev-genet-011112-112140.
4. **Radolf JD, Caimano MJ, Stevenson B, Hu LT.** 2012. Of ticks, mice and men: understanding the dual-host lifestyle of Lyme disease spirochaetes. Nat Rev Microbiol **10:**87–99. http://dx.doi.org/10.1038/nrmicro2714.
5. **Groshong AM, Blevins JS.** 2014. Insights into the biology of *Borrelia burgdorferi* gained through the application of molecular genetics. Adv Appl Microbiol **86:**41–143. http://dx.doi.org/10.1016/B978-0-12-800262-9.00002-0.
6. **Zhang L, Zhang Y, Adusumilli S, Liu L, Narasimhan S, Dai J, Zhao YO, Fikrig E.** 2011. Molecular interactions that enable movement of the Lyme disease agent from the tick gut into the hemolymph. PLoS Pathog **7:**e1002079. http://dx.doi.org/10.1371/journal.ppat.1002079.
7. **Dunham-Ems SM, Caimano MJ, Pal U, Wolgemuth CW, Eggers CH, Balic A, Radolf JD.** 2009. Live imaging reveals a biphasic mode of dissemination of *Borrelia burgdorferi* within ticks. J Clin Investig **119:**3652–3665. http://dx.doi.org/10.1172/JCI39401.
8. **Coburn J, Leong J, Chaconas G.** 2013. Illuminating the roles of the *Borrelia burgdorferi* adhesins. Trends Microbiol **21:**372–379. http://dx.doi.org/10.1016/j.tim.2013.06.005.
9. **Bockenstedt LK, Gonzalez D, Mao J, Li M, Belperron AA, Haberman A.** 2014. What ticks do under your skin: two-photon intravital imaging of *Ixodes scapularis* feeding in the presence of the Lyme disease spirochete. Yale J Biol Med **87:**3–13.
10. **Charon NW, Goldstein SF.** 2002. Genetics of motility and chemotaxis of a fascinating group of bacteria: the spirochetes. Annu Rev Genet **36:**47–73. http://dx.doi.org/10.1146/annurev.genet.36.041602.134359.
11. **Charon NW, Cockburn A, Li C, Liu J, Miller KA, Miller MR, Motaleb MA, Wolgemuth CW.** 2012. The unique paradigm of spirochete motility and chemotaxis. Annu Rev Microbiol **66:**349–370. http://dx.doi.org/10.1146/annurev-micro-092611-150145.
12. **Li C, Xu H, Zhang K, Liang FT.** 2010. Inactivation of a putative flagellar

motor switch protein FliG1 prevents *Borrelia burgdorferi* from swimming in highly viscous media and blocks its infectivity. Mol Microbiol **75:**1563–1576. http://dx.doi.org/10.1111/j.1365-2958.2010.07078.x.

13. **Sze CW, Zhang K, Kariu T, Pal U, Li C.** 2012. *Borrelia burgdorferi* needs chemotaxis to establish infection in mammals and to accomplish its enzootic cycle. Infect Immun **80:**2485–2492. http://dx.doi.org/10.1128/IAI.00145-12.
14. **Sultan SZ, Manne A, Stewart PE, Bestor A, Rosa PA, Charon NW, Motaleb MA.** 2013. Motility is crucial for the infectious life cycle of *Borrelia burgdorferi*. Infect Immun **81:**2012–2021. http://dx.doi.org/10.1128/IAI.01228-12.
15. **Malawista SE, de Boisfleury CA.** 2008. Clocking the Lyme spirochete. PLoS One **3:**e1633. http://dx.doi.org/10.1371/journal.pone.0001633.
16. **Ng LG, Hsu A, Mandell MA, Roediger B, Hoeller C, Mrass P, Iparraguirre A, Cavanagh LL, Triccas JA, Beverley SM, Scott P, Weninger W.** 2008. Migratory dermal dendritic cells act as rapid sensors of protozoan parasites. PLoS Pathog **4:**e1000222. http://dx.doi.org/10.1371/journal.ppat.1000222.
17. **Kojima S, Blair DF.** 2004. The bacterial flagellar motor: structure and function of a complex molecular machine. Int Rev Cytol **233:**93–134. http://dx.doi.org/10.1016/S0074-7696(04)33003-2.
18. **Khan S, Dapice M, Reese TS.** 1988. Effects of *mot* gene expression on the structure of the flagellar motor. J Mol Biol **202:**575–584. http://dx.doi.org/10.1016/0022-2836(88)90287-2.
19. **Blair DF, Berg HC.** 1988. Restoration of torque in defective flagellar motors. Science **242:**1678–1681. http://dx.doi.org/10.1126/science.2849208.
20. **Braun TF, Blair DF.** 2001. Targeted disulfide cross-linking of the MotB protein of *Escherichia coli*: evidence for two H(+) channels in the stator complex. Biochemistry **40:**13051–13059. http://dx.doi.org/10.1021/bi011264g.
21. **Izard J, Renken C, Hsieh CE, Desrosiers DC, Dunham-Ems S, La Vake C, Gebhardt LL, Limberger RJ, Cox DL, Marko M, Radolf JD.** 2009. Cryo-electron tomography elucidates the molecular architecture of *Treponema pallidum*, the syphilis spirochete. J Bacteriol **191:**7566–7580. http://dx.doi.org/10.1128/JB.01031-09.
22. **Zhao X, Norris SJ, Liu J.** 2014. Molecular architecture of bacterial flagellar motor in cells. Biochemistry **53:**4323–4333. http://dx.doi.org/10.1021/bi500059y.
23. **Chen S, Beeby M, Murphy GE, Leadbetter JR, Hendrixson DR, Briegel A, Li Z, Shi J, Tocheva EI, Muller A, Dobro MJ, Jensen GJ.** 2011. Structural diversity of bacterial flagellar motors. EMBO J **30:**2972–2981. http://dx.doi.org/10.1038/emboj.2011.186.
24. **Zhao X, Zhang K, Boquoi T, Hu B, Motaleb MA, Miller KA, James ME, Charon NW, Manson MD, Norris SJ, Li C, Liu J.** 2013. Cryoelectron tomography reveals the sequential assembly of bacterial flagella in *Borrelia burgdorferi*. Proc Natl Acad Sci U S A **110:**14390–14395. http://dx.doi.org/10.1073/pnas.1308306110.
25. **Chevance FF, Hughes KT.** 2008. Coordinating assembly of a bacterial macromolecular machine. Nat Rev Microbiol **6:**455–465. http://dx.doi.org/10.1038/nrmicro1887.
26. **Aldridge P, Hughes KT.** 2002. Regulation of flagellar assembly. Curr Opin Microbiol **5:**160–165. http://dx.doi.org/10.1016/S1369-5274(02)00302-8.
27. **Liu J, Lin T, Botkin DJ, McCrum E, Winkler H, Norris SJ.** 2009. Intact flagellar motor of *Borrelia burgdorferi* revealed by cryo-electron tomography: evidence for stator ring curvature and rotor/C-ring assembly flexion. J Bacteriol **191:**5026–5036. http://dx.doi.org/10.1128/JB.00340-09.
28. **Dombrowski C, Kan W, Motaleb MA, Charon NW, Goldstein RE, Wolgemuth CW.** 2009. The elastic basis for the shape of *Borrelia burgdorferi*. Biophys J **96:**4409–4417. http://dx.doi.org/10.1016/j.bpj.2009.02.066.
29. **Li C, Bakker RG, Motaleb MA, Sartakova ML, Cabello FC, Charon NW.** 2002. Asymmetrical flagellar rotation in *Borrelia burgdorferi* nonchemotactic mutants. Proc Natl Acad Sci U S A **99:**6169–6174. http://dx.doi.org/10.1073/pnas.092010499.
30. **Kudryashev M, Cyrklaff M, Baumeister W, Simon MM, Wallich R, Frischknecht F.** 2009. Comparative cryo-electron tomography of pathogenic Lyme disease spirochetes. Mol Microbiol **71:**1415–1434. http://dx.doi.org/10.1111/j.1365-2958.2009.06613.x.
31. **Sze CW, Morado DR, Liu J, Charon NW, Xu H, Li C.** 2011. Carbon storage regulator A ($CsrA_{Bb}$) is a repressor of *Borrelia burgdorferi* flagellin protein FlaB. Mol Microbiol **82:**851–864. http://dx.doi.org/10.1111/j.1365-2958.2011.07853.x.
32. **Charon NW, Goldstein SF, Marko M, Hsieh C, Gebhardt LL, Motaleb MA, Wolgemuth CW, Limberger RJ, Rowe N.** 2009. The flat ribbon configuration of the periplasmic flagella of *Borrelia burgdorferi* and its relationship to motility and morphology. J Bacteriol **191:**600–607. http://dx.doi.org/10.1128/JB.01288-08.
33. **Motaleb MA, Corum L, Bono JL, Elias AF, Rosa P, Samuels DS, Charon NW.** 2000. *Borrelia burgdorferi* periplasmic flagella have both skeletal and motility functions. Proc Natl Acad Sci U S A **97:**10899–10904. http://dx.doi.org/10.1073/pnas.200221797.
34. **Sartakova ML, Dobrikova EY, Motaleb MA, Godfrey HP, Charon NW, Cabello FC.** 2001. Complementation of a nonmotile *flaB* mutant of *Borrelia burgdorferi* by chromosomal integration of a plasmid containing a wild-type *flaB* allele. J Bacteriol **183:**6558–6564. http://dx.doi.org/10.1128/JB.183.22.6558-6564.2001.
35. **Wolgemuth CW, Charon NW, Goldstein SF, Goldstein RE.** 2006. The flagellar cytoskeleton of the spirochetes. J Mol Microbiol Biotechnol **11:**221–227. http://dx.doi.org/10.1159/000094056.
36. **Botkin DJ, Abbott AN, Stewart PE, Rosa PA, Kawabata H, Watanabe H, Norris SJ.** 2006. Identification of potential virulence determinants by Himar1 transposition of infectious *Borrelia burgdorferi* B31. Infect Immun **74:**6690–6699. http://dx.doi.org/10.1128/IAI.00993-06.
37. **Lin T, Gao L, Zhang C, Odeh E, Jacobs MB, Coutte L, Chaconas G, Philipp MT, Norris SJ.** 2012. Analysis of an ordered, comprehensive STM mutant library in infectious *Borrelia burgdorferi*: insights into the genes required for mouse infectivity. PLoS One **7:**e47532. http://dx.doi.org/10.1371/journal.pone.0047532.
38. **Vijay-Kumar M, Gewirtz AT.** 2009. Flagellin: key target of mucosal innate immunity. Mucosal Immunol **2:**197–205. http://dx.doi.org/10.1038/mi.2009.9.
39. **Honko AN, Mizel SB.** 2005. Effects of flagellin on innate and adaptive immunity. Immunol Res **33:**83–101. http://dx.doi.org/10.1385/IR:33:1:083.
40. **Newton SMC, Joys TM, Anderson SA, Kennedy RC, Hovi ME, Stocker BAD.** 1995. Expression and immunogenicity of an 18-residue epitope of HIV1 gp41 inserted in the flagellar protein of a *Salmonella* live vaccine. Res Microbiol **146:**203–216. http://dx.doi.org/10.1016/0923-2508(96)80276-2.
41. **Harada H, Nishikawa F, Higashi N, Kita E.** 2002. Development of a mucosal complex vaccine against oral Salmonella infection in mice. Microbiol Immunol **46:**891–905. http://dx.doi.org/10.1111/j.1348-0421.2002.tb02778.x.
42. **Kirkpatrick BD, Tenney KM, Larsson CJ, O'Neill JP, Ventrone C, Bentley M, Upton A, Hindle Z, Fidler C, Kutzko D, Holdridge R, LaPointe C, Hamlet S, Chatfield SN.** 2005. The novel oral typhoid vaccine M01ZH09 is well tolerated and highly immunogenic in 2 vaccine presentations. J Infect Dis **192:**360–366. http://dx.doi.org/10.1086/431605.
43. **Barbour AG, Jasinskas A, Kayala MA, Davies DH, Steere AC, Baldi P, Felgner PL.** 2008. A genome-wide proteome array reveals a limited set of immunogens in natural infections of humans and white-footed mice with *Borrelia burgdorferi*. Infect Immun **76:**3374–3389. http://dx.doi.org/10.1128/IAI.00048-08.
44. **Barthold SW.** 1999. Specificity of infection-induced immunity among *Borrelia burgdorferi* sensu lato species. Infect Immun **67:**36–42.
45. **Rego RO, Bestor A, Rosa PA.** 2011. Defining the plasmid-encoded restriction-modification systems of the Lyme disease spirochete *Borrelia burgdorferi*. J Bacteriol **193:**1161–1171. http://dx.doi.org/10.1128/JB.01176-10.
46. **Elias AF, Stewart PE, Grimm D, Caimano MJ, Eggers CH, Tilly K, Bono JL, Akins DR, Radolf JD, Schwan TG, Rosa P.** 2002. Clonal polymorphism of *Borrelia burgdorferi* strain B31 MI: implications for mutagenesis in an infectious strain background. Infect Immun **70:**2139–2150. http://dx.doi.org/10.1128/IAI.70.4.2139-2150.2002.
47. **Fraser CM, Casjens S, Huang WM, Sutton GG, Clayton R, Lathigra R, White O, Ketchum KA, Dodson R, Hickey EK, Gwinn M, Dougherty B, Tomb JF, Fleischmann RD, Richardson D, Peterson J, Kerlavage AR, Quackenbush J, Salzberg S, Hanson M, van Vugt R, Palmer N, Adams MD, Gocayne J.** 1997. Genomic sequence of a Lyme disease spirochaete, *Borrelia burgdorferi*. Nature **390:**580–586. http://dx.doi.org/10.1038/37551.
48. **Motaleb MA, Miller MR, Bakker RG, Li C, Charon NW.** 2007. Isolation and characterization of chemotaxis mutants of the Lyme disease spirochete *Borrelia burgdorferi* using allelic exchange mutagenesis, flow cytometry, and cell tracking. Methods Enzymol **422:**421–437. http://dx.doi.org/10.1016/S0076-6879(06)22021-4.
49. **Motaleb MA, Pitzer JE, Sultan SZ, Liu J.** 2011. A novel gene inactivation system reveals an altered periplasmic flagellar orientation in a *Borrelia*

burgdorferi fliL mutant. J Bacteriol **193:**3324–3331. http://dx.doi.org/10.1128/JB.00202-11.
50. **Elias AF, Bono JL, Kupko JJ, III, Stewart PE, Krum JG, Rosa PA.** 2003. New antibiotic resistance cassettes suitable for genetic studies in *Borrelia burgdorferi*. J Mol Microbiol Biotechnol **6:**29–40. http://dx.doi.org/10.1159/000073406.
51. **Bono JL, Elias AF, Kupko JJ, III, Stevenson B, Tilly K, Rosa P.** 2000. Efficient targeted mutagenesis in *Borrelia burgdorferi*. J Bacteriol **182:**2445–2452. http://dx.doi.org/10.1128/JB.182.9.2445-2452.2000.
52. **Ge Y, Old IG, Saint Girons I, Charon NW.** 1997. Molecular characterization of a large *Borrelia burgdorferi* motility operon which is initiated by a consensus σ^{70} promoter. J Bacteriol **179:**2289–2299.
53. **Carroll JA, El Hage N, Miller JC, Babb K, Stevenson B.** 2001. *Borrelia burgdorferi* RevA antigen is a surface-exposed outer membrane protein whose expression is regulated in response to environmental temperature and pH. Infect Immun **69:**5286–5293. http://dx.doi.org/10.1128/IAI.69.9.5286-5293.2001.
54. **Kremer JR, Mastronarde DN, McIntosh JR.** 1996. Computer visualization of three-dimensional image data using IMOD. J Struct Biol **116:**71–76. http://dx.doi.org/10.1006/jsbi.1996.0013.
55. **Pitzer JE, Sultan SZ, Hayakawa Y, Hobbs G, Miller MR, Motaleb MA.** 2011. Analysis of the *Borrelia burgdorferi* cyclic-di-GMP binding protein PlzA reveals a role in motility and virulence. Infect Immun **79:**1815–1825. http://dx.doi.org/10.1128/IAI.00075-11.
56. **Sultan SZ, Pitzer JE, Boquoi T, Hobbs G, Miller MR, Motaleb MA.** 2011. Analysis of the HD-GYP domain cyclic-di-GMP phosphodiesterase reveals a role in motility and enzootic life cycle of *Borrelia burgdorferi*. Infect Immun **79:**3273–3283. http://dx.doi.org/10.1128/IAI.05153-11.
57. **Sultan SZ, Pitzer JE, Miller MR, Motaleb MA.** 2010. Analysis of a *Borrelia burgdorferi* phosphodiesterase demonstrates a role for cyclic-di-guanosine monophosphate in motility and virulence. Mol Microbiol **77:**128–142. http://dx.doi.org/10.1111/j.1365-2958.2010.07191.x.
58. **Ma Y, Seiler KP, Eichwald EJ, Weis JH, Teuscher C, Weis JJ.** 1998. Distinct characteristics of resistance to *Borrelia burgdorferi* induced arthritis in C57BL/6N mice. Infect Immun **66:**161–168.
59. **Weis JJ, McCracken BA, Ma Y, Fairbairn D, Roper RJ, Morrison TB, Weis JH, Zachary JF, Doerge RW, Teuscher C.** 1999. Identification of quantitative trait loci governing arthritis severity and humoral responses in the murine model of Lyme disease. J Immunol **162:**948–956.
60. **Brown JP, Zachary JF, Teuscher C, Weis JJ, Wooten RM.** 1999. Dual role of interleukin-10 in murine Lyme disease: regulation of arthritis severity and host defense. Infect Immun **67:**5142–5150.
61. **Stewart PE, Rosa PA.** 2008. Transposon mutagenesis of the Lyme disease agent *Borrelia burgdorferi*. Methods Mol Biol **431:**85–95.
62. **Policastro PF, Schwan TG.** 2003. Experimental infection of *Ixodes scapularis* larvae (Acari: Ixodidae) by immersion in low passage cultures of *Borrelia burgdorferi*. J Med Entomol **40:**364–370. http://dx.doi.org/10.1603/0022-2585-40.3.364.
63. **Mulay VB, Caimano MJ, Iyer R, Dunham-Ems S, Liveris D, Petzke MM, Schwartz I, Radolf JD.** 2009. *Borrelia burgdorferi bba74* is expressed exclusively during tick feeding and is regulated by both arthropod- and mammalian host-specific signals. J Bacteriol **191:**2783–2794. http://dx.doi.org/10.1128/JB.01802-08.
64. **Patton TG, Dietrich G, Dolan MC, Piesman J, Carroll JA, Gilmore RD, Jr.** 2011. Functional analysis of the *Borrelia burgdorferi bba64* gene product in murine infection via tick infestation. PLoS One **6:**e19536. http://dx.doi.org/10.1371/journal.pone.0019536.
65. **Wooten RM, Ma Y, Yoder RA, Brown JP, Weis JH, Zachary JF, Kirschning CJ, Weis JJ.** 2002. Toll-like receptor 2 is required for innate, but not acquired, host defense to *Borrelia burgdorferi*. J Immunol **168:**348–355. http://dx.doi.org/10.4049/jimmunol.168.1.348.
66. **Lazarus JJ, McCarter AL, Neifer-Sadhwani K, Wooten RM.** 2012. ELISA-based measurement of antibody responses and PCR-based detection profiles can distinguish between active infection and early clearance of *Borrelia burgdorferi*. Clin Dev Immunol **2012:**138069. http://dx.doi.org/10.1155/2012/138069.
67. **Andermann TM, Chen YT, Ottemann KM.** 2002. Two predicted chemoreceptors of *Helicobacter pylori* promote stomach infection. Infect Immun **70:**5877–5881. http://dx.doi.org/10.1128/IAI.70.10.5877-5881.2002.
68. **Bian J, Fenno JC, Li C.** 2012. Development of a modified gentamicin resistance cassette for genetic manipulation of the oral spirochete *Treponema denticola*. Appl Environ Microbiol **78:**2059–2062. http://dx.doi.org/10.1128/AEM.07461-11.
69. **Van Way SM, Hosking ER, Braun TF, Manson MD.** 2000. Mot protein assembly into the bacterial flagellum: a model based on mutational analysis of the *motB* gene. J Mol Biol **297:**7–24. http://dx.doi.org/10.1006/jmbi.2000.3548.
70. **Muramoto K, Macnab RM.** 1998. Deletion analysis of MotA and MotB, components of the force-generating unit in the flagellar motor of *Salmonella*. Mol Microbiol **29:**1191–1202. http://dx.doi.org/10.1046/j.1365-2958.1998.00998.x.
71. **Motaleb MA, Sal MS, Charon NW.** 2004. The decrease in FlaA observed in a *flaB* mutant of *Borrelia burgdorferi* occurs posttranscriptionally. J Bacteriol **186:**3703–3711. http://dx.doi.org/10.1128/JB.186.12.3703-3711.2004.
72. **Piesman J.** 1993. Standard system for infecting ticks (Acari: Ixodidae) with the Lyme disease spirochete, *Borrelia burgdorferi*. J Med Entomol **30:**199–203. http://dx.doi.org/10.1093/jmedent/30.1.199.
73. **Crippa M, Rais O, Gern L.** 2002. Investigations on the mode and dynamics of transmission and infectivity of *Borrelia burgdorferi* sensu stricto and *Borrelia afzelii* in *Ixodes ricinus* ticks. Vector Borne Zoonotic Dis **2:**3–9. http://dx.doi.org/10.1089/153036602760260724.
74. **Zhou JD, Blair DF.** 1997. Residues of the cytoplasmic domain of MotA essential for torque generation in the bacterial flagellar motor. J Mol Biol **273:**428–439. http://dx.doi.org/10.1006/jmbi.1997.1316.
75. **Motaleb MA, Sultan SZ, Miller MR, Li C, Charon NW.** 2011. CheY3 of *Borrelia burgdorferi* is the key response regulator essential for chemotaxis and forms a long-lived phosphorylated intermediate. J Bacteriol **193:**3332–3341. http://dx.doi.org/10.1128/JB.00362-11.
76. **Motaleb MA, Miller MR, Li C, Bakker RG, Goldstein SF, Silversmith RE, Bourret RB, Charon NW.** 2005. CheX is a phosphorylated CheY phosphatase essential for *Borrelia burgdorferi* chemotaxis. J Bacteriol **187:**7963–7969. http://dx.doi.org/10.1128/JB.187.23.7963-7969.2005.
77. **Kennedy MJ, Rosey EL, Yancey RJ, Jr.** 1997. Characterization of *flaA*$^-$ and *flaB*$^-$ mutants of *Serpulina hyodysenteriae*: both flagellin subunits, FlaA and FlaB, are necessary for full motility and intestinal colonization. FEMS Microbiol Lett **153:**119–128. http://dx.doi.org/10.1016/S0378-1097(97)00244-9.
78. **Rosey EL, Kennedy MJ, Yancey RJ, Jr.** 1996. Dual *flaA1 flaB1* mutant of *Serpulina hyodysenteriae* expressing periplasmic flagella is severely attenuated in a murine model of swine dysentery. Infect Immun **64:**4154–4162.
79. **Lambert A, Picardeau M, Haake DA, Sermswan RW, Srikram A, Adler B, Murray GA.** 2012. FlaA proteins in *Leptospira interrogans* are essential for motility and virulence but are not required for formation of the flagellum sheath. Infect Immun **80:**2019–2025. http://dx.doi.org/10.1128/IAI.00131-12.
80. **Guyard C, Raffel SJ, Schrumpf ME, Dahlstrom E, Sturdevant D, Ricklefs SM, Martens C, Hayes SF, Fischer ER, Hansen BT, Porcella SF, Schwan TG.** 2013. Periplasmic flagellar export apparatus protein, FliH, is involved in post-transcriptional regulation of FlaB, motility and virulence of the relapsing fever spirochete *Borrelia hermsii*. PLoS One **8:**e72550. http://dx.doi.org/10.1371/journal.pone.0072550.
81. **Mathur R, Oh H, Zhang D, Park SG, Seo J, Koblansky A, Hayden MS, Ghosh S.** 2012. A mouse model of *Salmonella typhi* infection. Cell **151:**590–602. http://dx.doi.org/10.1016/j.cell.2012.08.042.
82. **Hayashi F, Smith KD, Ozinsky A, Hawn TR, Yi EC, Goodlett DR, Eng JK, Akira S, Underhill DM, Aderem A.** 2001. The innate immune response to bacterial flagellin is mediated by Toll-like receptor 5. Nature **410:**1099–1103. http://dx.doi.org/10.1038/35074106.
83. **Eaton KA, Morgan DR, Krakowka S.** 1992. Motility as a factor in the colonisation of gnotobiotic piglets by *Helicobacter pylori*. J Med Microbiol **37:**123–127. http://dx.doi.org/10.1099/00222615-37-2-123.
84. **Josenhans C, Ferrero RL, Labigne A, Suerbaum S.** 1999. Cloning and allelic exchange mutagenesis of two flagellin genes of *Helicobacter felis*. Mol Microbiol **33:**350–362. http://dx.doi.org/10.1046/j.1365-2958.1999.01478.x.
85. **Ottemann KM, Lowenthal AC.** 2002. *Helicobacter pylori* uses motility for initial colonization and to attain robust infection. Infect Immun **70:**1984–1990. http://dx.doi.org/10.1128/IAI.70.4.1984-1990.2002.
86. **Josenhans C, Suerbaum S.** 2002. The role of motility as a virulence factor in bacteria. Int J Med Microbiol **291:**605–614. http://dx.doi.org/10.1078/1438-4221-00173.
87. **Lovell MA, Barrow PA.** 1999. Intestinal colonisation of gnotobiotic pigs by Salmonella organisms: interaction between isogenic and unrelated

strains. J Med Microbiol **48:**907–916. http://dx.doi.org/10.1099/00222615-48-10-907.
88. **Butler SM, Camilli A.** 2005. Going against the grain: chemotaxis and infection in *Vibrio cholerae*. Nat Rev Microbiol **3:**611–620. http://dx.doi.org/10.1038/nrmicro1207.
89. **Cossart P, Sansonetti PJ.** 2004. Bacterial invasion: the paradigms of enteroinvasive pathogens. Science **304:**242–248. http://dx.doi.org/10.1126/science.1090124.
90. **Young GM, Badger JL, Miller VL.** 2000. Motility is required to initiate host cell invasion by *Yersinia enterocolitica*. Infect Immun **68:**4323–4326. http://dx.doi.org/10.1128/IAI.68.7.4323-4326.2000.
91. **Lee A, O'Rourke JL, Barrington PJ, Trust TJ.** 1986. Mucus colonization as a determinant of pathogenicity in intestinal infection by *Campylobacter jejuni*: a mouse cecal model. Infect Immun **51:**536–546.
92. **Lazarus JJ, Meadows MJ, Lintner RE, Wooten RM.** 2006. IL-10 deficiency promotes increased Borrelia burgdorferi clearance predominantly through enhanced innate immune responses. J Immunol **177:**7076–7085. http://dx.doi.org/10.4049/jimmunol.177.10.7076.
93. **Sonenshine DE, Hynes WL.** 2008. Molecular characterization and related aspects of the innate immune response in ticks. Front Biosci **13:**7046–7063.
94. **Fikrig E, Narasimhan S.** 2006. Borrelia burgdorferi–traveling incognito? Microbes Infect **8:**1390–1399. http://dx.doi.org/10.1016/j.micinf.2005.12.022.
95. **Hajdusek O, Sima R, Ayllon N, Jalovecka M, Perner J, de la Fuente J, Kopacek P.** 2013. Interaction of the tick immune system with transmitted pathogens. Front Cell Infect Microbiol **3:**26. http://dx.doi.org/10.3389/fcimb.2013.00026.
96. **Sal MS, Li C, Motaleb MA, Shibata S, Aizawa S, Charon NW.** 2008. *Borrelia burgdorferi* uniquely regulates its motility genes and has an intricate flagellar hook-basal body structure. J Bacteriol **190:**1912–1921. http://dx.doi.org/10.1128/JB.01421-07.
97. **Pal U, Li X, Wang T, Montgomery RR, Ramamoorthi N, Desilva AM, Bao F, Yang X, Pypaert M, Pradhan D, Kantor FS, Telford S, Anderson JF, Fikrig E.** 2004. TROSPA, an *Ixodes scapularis* receptor for *Borrelia burgdorferi*. Cell **119:**457–468. http://dx.doi.org/10.1016/j.cell.2004.10.027.